

Random Walks and Anderson Localisation in a Three-Dimensional Class C Network Model

M. Ortuño, and A. M. Somoza

Departamento de Física, Universidad de Murcia, Murcia 30.071, Spain

J. T. Chalker

Theoretical Physics, Oxford University, 1, Keble Road, Oxford, OX1 3NP, United Kingdom

(Dated: October 23, 2018)

We study the disorder-induced localisation transition in a three-dimensional network model that belongs to symmetry class C. The model represents quasiparticle dynamics in a gapless spin-singlet superconductor without time-reversal invariance. It is a special feature of network models with this symmetry that the conductance and density of states can be expressed as averages in a classical system of dense, interacting random walks. Using this mapping, we present a more precise numerical study of critical behaviour at an Anderson transition than has been possible previously in any context.

PACS numbers: 72.15.Rn 64.60.De 05.40.Fb

Anderson transitions between diffusive and localised phases of quantum particles in disordered systems constitute an important category of critical phenomena. Depending on dimensionality and the symmetries of the Hamiltonian, various universality classes are possible for scaling behaviour [1]. In most cases there is no known connection between these Anderson universality classes and those for phase transitions in classical systems, but in a special instance, known as class C, properties of suitably chosen quantum lattice models can be expressed in terms of observables for a classical model defined on the same lattice. This mapping was originally discovered in the context of the spin quantum Hall effect, where it relates a delocalisation transition in two dimensions to classical percolation, also in two dimensions, for which many relevant aspects of critical behaviour are known exactly [2]. In this paper we apply the mapping to a three-dimensional system for which the classical counterpart is a model of interacting random walks [3]. The classical model is of interest both as a representation of the quantum problem and in its own right. While no exact results for its behaviour are available, the mapping makes possible simulations of the Anderson transition with unprecedented precision.

The symmetry class for localisation that we are concerned with is one of seven recognised about a decade ago as being additional to the three Wigner-Dyson classes that were originally identified in the context of random matrix theory [4]. Systems in these additional symmetry classes are distinguished from ones in the Wigner-Dyson classes by having a special point in the energy spectrum and energy levels that appear in pairs either side of this point. In particular, models in class C arise from the Bogoliubov de-Gennes Hamiltonian for quasiparticles in a gapless, disordered spin-singlet superconductor with broken time-reversal symmetry for orbital motion but negligible Zeeman splitting. Here the special energy is the chemical potential (which we set to zero) and pairs of levels are related by particle-hole symmetry. Quasiparticle states in a three-dimensional system of this type have an Anderson transition as a function of disorder strength, which must be probed via spin or thermal transport since charge transport is

short-circuited by the condensate. Particle-hole symmetry has profound consequences for the influence of disorder on quasiparticle eigenstates and for the Anderson transition, which have been explored previously using random matrix theory [4], the non-linear sigma model [5, 6], and via calculations for one-dimensional systems [7]. Most importantly, the density of states at the chemical potential plays the role of an order parameter for the transition, being finite in the metal and zero in the insulator; by contrast, the density of states shows no critical behaviour at transitions in the Wigner-Dyson classes.

The quantum to classical mapping provides a framework within which quasiparticle properties can be studied in great detail starting from a simplified description of a disordered superconductor. It is based on a formulation of the localisation problem as a network model [8] in which quasiparticles propagate along the directed links of a lattice and scatter between links at nodes. Disorder enters the model in the form of quenched random phase shifts associated with propagation on links. For versions of the network model belonging to class C, first introduced in Ref. [9], the disorder-averaged quasiparticle density of states and (spin) conductance can be expressed as averages over configurations of interacting classical random walks on the same directed lattice [2, 3]. This relation between quantum properties and classical walks holds on any graph in which all nodes have exactly two incoming and two outgoing links. A single parameter p controls behaviour at nodes: incoming and outgoing links are arranged in pairs, and a particle passing through the node follows the pairing with probability p , or switches with probability $1 - p$. More precisely, in the quantum problem the probabilities calculated by squaring amplitudes in the scattering matrix for the node take the values p and $1 - p$, while in the classical problem the connection at each node between ingoing and outgoing links is a quenched random variable having two possible arrangements with these probabilities. Given a directed graph with the required coordination, any choice of classical connections at the nodes separates paths on the graph into a set of distinct, closed, mutually avoiding walks. Average properties of these walks are calculated from a sum over all node configurations,

weighted according to their probabilities.

To use the mapping for a three-dimensional model one must select a four-fold coordinated lattice, assign directions to the links so that two are incoming and two are outgoing at every node, and pair incoming with outgoing links. We pick the diamond lattice and choose link directions and pairings at nodes so that the system has localised states at $p = 0$ and extended states at $p = 1$. The resulting unit cell contains 24 sites and we defer a full description until later in this paper. We study samples consisting of $L \times L \times L$ unit cells with two alternative sets of boundary conditions: using the classical mapping, we calculate conductance between two opposite, open faces (with periodic boundary conditions in the other directions), and we calculate the density of states in closed samples with periodic boundary conditions in all three directions.

The results of the mapping are as follows [3]. First, the disorder-averaged spin conductance $G(p, L)$ of the quantum system is given (in units of $\hbar/4\pi$) by the average of the number N_L of classical paths from a specified open face to the other. Second, the average density of states $\rho(\varepsilon)$ for eigenphases of a unitary time evolution operator, which occupy the range $-\pi \leq \varepsilon \leq \pi$ and play the role of energy levels, is given in terms of the probability $P(s, p)$ in the classical problem for a given link to belong to a closed walk of length s steps, by

$$\rho(\varepsilon, p) = (2\pi)^{-1} \left[1 - \sum_{s>0} P(s, p) \cos(2s\varepsilon) \right]. \quad (1)$$

In the following we present and analyse data for $G(p, L)$ and $P(s, p)$, and deduce from the latter the critical properties of $\rho(\varepsilon, p)$. In addition, we study the mean square end-to-end distance $\langle R(s)^2 \rangle$ of walks as a function of number of steps s . This last quantity has no direct significance for the original quantum problem but provides a useful characterisation of the classical walks.

We can study much larger systems using the classical description than is possible for a quantum Hamiltonian with disorder: we use sizes in the range $40 \leq L \leq 440$, and calculate averages over 10^7 realisations for the smallest samples and 4×10^3 for the largest. The biggest systems hence contain over $2 \cdot 10^9$ sites in total, and over 10^6 sites in cross-section. By contrast, direct calculations of eigenfunctions using sparse matrix techniques [10, 11, 12] are limited to systems 10^2 or 10^3 times smaller, while high precision studies of Anderson transitions [13] using transfer matrix methods [14] are restricted to systems with a cross-section of around 10^3 sites. Our system sizes enable us to determine the values of critical exponents with about an order of magnitude higher precision than has been possible numerically for other Anderson transitions.

We discuss first our data for conductance $G(p, L)$. Our measurements span the range $0.25 \leq p \leq 0.28$ and yield values for $G(p, L)$ in the metal with statistical uncertainties of less than 0.1%, except for the largest sample size ($L = 440$) where they are 0.4%. The model is designed to have a critical point at $p = p_c$ separating a metallic phase for $p > p_c$ from

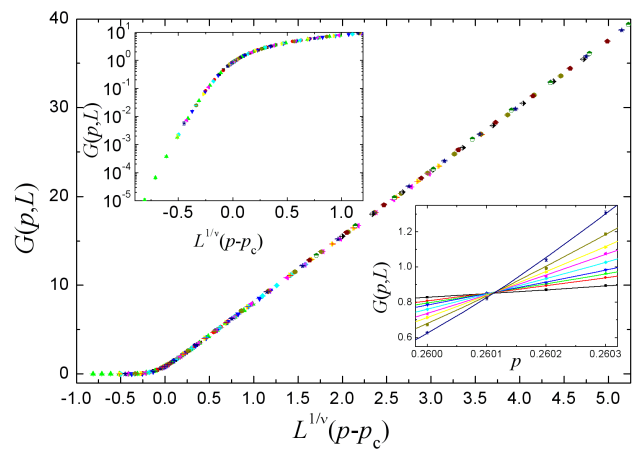


FIG. 1: (Color online) Conductance as a function of $(p - p_c)L^{1/\nu}$, illustrating scaling collapse. Upper inset: same data on a logarithmic conductance scale. Lower inset: conductance as a function of p for several values of L . Lines are scaling fit described in main text.

an insulating one for $p < p_c$. From Ohm's law the metallic phase is characterised by the behaviour $G(p, L) \sim \sigma(p)L$ for sufficiently large L , where $\sigma(p)$ is the conductivity, while in the insulator $G(p, L) \rightarrow 0$ at large L . Close to the critical point we expect one parameter scaling in the form

$$G(p, L) = f(L/\xi(p)), \quad (2)$$

where $\xi(p)$ is the localisation length in the insulator and the correlation length in the metal. Hence curves of $G(p, L)$ as a function of p for different L intersect at p_c , as illustrated in the lower inset to Fig. 1. In addition, assuming that $\xi(p)$ diverges at the transition as $\xi(p) \propto |p - p_c|^{-\nu}$, data for $G(p, L)$ in the critical regime should collapse onto a single curve when plotted as a function of $x \equiv (p - p_c)L^{1/\nu}$. This collapse is shown in Fig. 1 using a linear scale for $G(p, L)$, and in the upper left inset using a logarithmic scale to display more clearly behaviour in the insulator.

Our estimates for the values of ν and p_c obtained from such a scaling analysis are

$$\nu = 0.9985 \pm 0.0015 \quad (3)$$

and $p_c = 0.260116 \pm 0.000002$. The analysis in detail is as follows. Extending Eq. (2) to include corrections to scaling, we expect

$$G(p, L) = \tilde{f}(L^{1/\nu}\phi, L^{y_{\text{irr}}}\psi), \quad (4)$$

where ϕ is the relevant scaling variable and ψ is the scaling variable for the leading correction, which is irrelevant provided $y_{\text{irr}} < 0$. Since $G(L, p)$ varies smoothly with p at fixed L , the scaling variables have Taylor expansions

$$\phi = (p - p_c) + A(p - p_c)^2 \dots \quad (5)$$

and $\psi = 1 + B(p - p_c) \dots$, in which leading coefficients have been fixed via the definition of $\tilde{f}(x, y)$. As a first step, we omit

all corrections to scaling, setting A and higher coefficients to zero and considering $\tilde{f}(x, 0)$. We construct this scaling function using cubic B-splines. We judge all fits by comparing the value of χ^2 with the number of degrees of freedom. For the splines we use 18 internal knot points at a spacing of 0.1 for $-0.5 \leq x \leq 1.0$, where curvature of $\tilde{f}(x, 0)$ is highest, and a spacing of 1 for $1 \leq x \leq 5$, where $\tilde{f}(x, 0)$ is almost linear in x . A coarser mesh of knot points does not allow an adequate fit to the data, while a finer one does not significantly improve the fit. Next we allow for an irrelevant scaling variable, by Taylor expanding $\tilde{f}(x, y)$ in y : we find that the form

$$\tilde{f}(x, y) = \tilde{f}(x, 0)[1 + Cy] \quad (6)$$

with $y_{\text{irr}} = -1$ and C constant provides an adequate description of the data. Finally, we allow for a non-linear scaling variable, as in Eq. (5), finding from the effect on χ^2 that non-zero A is justified but non-zero B or further terms are not.

Taking data with $p \leq p_{\text{max}} = 0.273$ (excluded values are far from the critical point) and $x \geq -0.5$ (excluded values are deep in the insulator, where errors in $G(L, p)$ are large), we have 262 points to fit and 26 parameters (the values of ν , p_c , A , C , 18 internal spline points and four boundary ones). Our fit has $\chi^2 = 236.4$ and is insensitive to the value of p_{max} in the range $0.265 \leq p_{\text{max}} \leq 0.28$. Since the fit yields a value for χ^2 close to the number of degrees of freedom, $262 - 26 = 236$, we believe that errors in our values for ν and p_c are due mainly to statistical errors in the data. We place 95% confidence limits on these values in two independent ways. In one we find the variation that increases χ^2 by 4. In the other we use a Monte Carlo technique to generate synthetic data [15]. The two methods give the same results.

Our value for ν is in striking, although presumably accidental, agreement with the leading order result from an ϵ expansion in $2 + \epsilon$ dimensions [5], $\nu = 1/\epsilon$, evaluated at $\epsilon = 1$. It is also consistent with the value $\nu \approx 0.9$ found in an earlier transfer matrix calculation [16] for a three-dimensional class C network model, which did not use the mapping to classical random walks and so was restricted to much smaller system sizes. The closeness of our value to $\nu = 1$ is tantalising but we are not aware of any theoretical reason to attach significance to this. Indeed, the upper critical dimension for the localisation transition in class C is believed to be four [17], and so non-trivial exponent values are expected in three dimensions.

We next present our data for the integrated return probability $N(s, p)$, which is related to $P(s, p)$ via

$$N(s, p) = \sum_{t \geq s} P(t, p). \quad (7)$$

From this we deduce the critical behaviour of the classical walks and of the quantum density of states. These data are obtained in closed samples by generating all walks for a given realisation of node configurations and averaging over different realisations, using sample sizes $L \leq 300$. In the critical regime walks are fractal with dimension d_f . The length $\xi(p)$ sets their characteristic size in the insulator, so that the characteristic arc length is $[\xi(p)]^{d_f}$; in the metal $\xi(p)$ represents

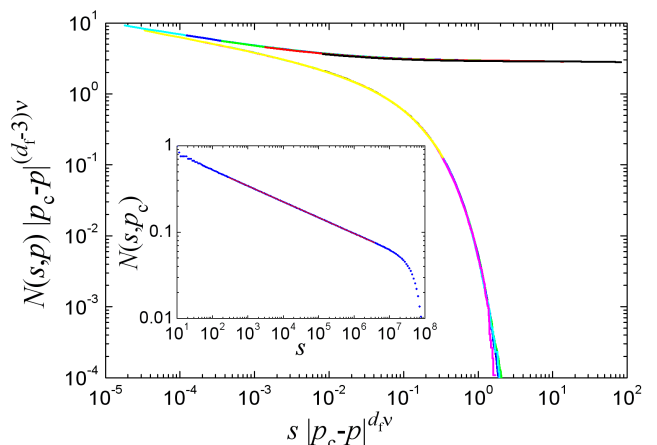


FIG. 2: (Color online) $|p - p_c|^{(d_f - 3)\nu} N(s, p)$ as a function of $s |p - p_c|^{d_f \nu}$ on double logarithmic scales for several values of p either side of p_c . Inset: $N(s, p_c)$ as a function of s on double logarithmic scales.

a crossover length beyond which scaling properties are as for free random walks. Close to the critical point we expect the scaling form

$$N(s, p) = \xi(p)^{d_f - 3} h_{\pm}(s/\xi(p)^{d_f}) \quad (8)$$

to hold, with scaling functions $h_+(x)$ for $p > p_c$ and $h_-(x)$ for $p < p_c$ that have distinct behaviour at large x but share the same power law form, $h(x) \sim x^{2-\tau}$, at small x . Since $N(s, p)$ should be independent of $\xi(p)$ at small s , we have the exponent relation

$$d_f = \frac{3}{\tau - 1}. \quad (9)$$

Data at $p = p_c$ are shown in the inset to Fig. 2: they confirm power law behaviour over six decades in s , yielding the exponent value

$$\tau = 2.184 \pm 0.003 \quad (10)$$

and hence $d_f = 2.534 \pm 0.009$. Using our values for d_f and ν , we demonstrate in the main panel of Fig. 2 scaling collapse following Eq. (8) for seven values of p in the insulator (0.250, 0.253, 0.255, 0.256, 0.257, 0.258, and 0.259) and five values in the metal (0.261, 0.262, 0.263, 0.265, and 0.270). We note the excellent overlap of data in each phase. Both scaling functions $h_{\pm}(x)$ follow the power-law behaviour of the critical point at small x . At large x , $h_-(x)$ falls off exponentially, while $h_+(x)$ tends to a constant: the escape probability.

These results can be combined with those of Ref. [3] to conclude for the quantum density of states that: (i) $\rho(\epsilon, p) \propto \epsilon^2$ in the insulator; (ii) $\rho(\epsilon, p_c) \propto |\epsilon|^{\tau-2}$ at the critical point; while in the metal (iii) $\rho(0, p) \propto (p - p_c)^{(3-d_f)\nu}$ and (iv) $[\rho(\epsilon, p) - \rho(0, p)] \propto |\epsilon|^{1/2}$. For comparison, the ϵ expansion gives [5] at leading order: $\rho(\epsilon, p_c) \propto |\epsilon|^{\epsilon/2}$ and $\rho(0, p) \propto (p - p_c)$.

To examine further the properties of classical walks at the critical point and in the metal we have calculated $\langle R(s)^2 \rangle$ for

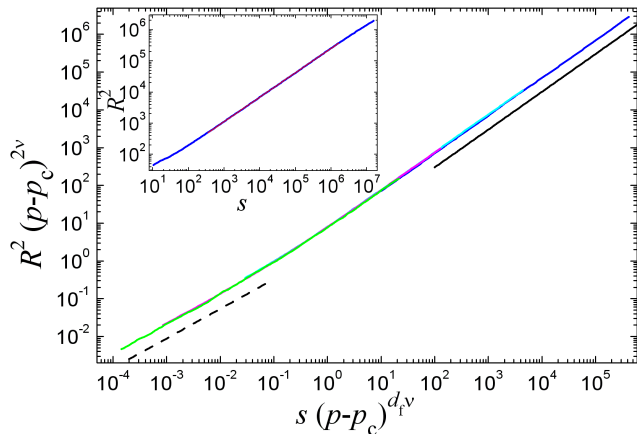


FIG. 3: (Color online) $\langle R^2(s) \rangle / \xi(p)^2$ as a function of $s / \xi(p)^{d_f}$ in the metal ($p = 0.265, 0.27, 0.3$ and 0.5), on double logarithmic scales. The continuous and dashed lines have gradients of 1 and $2/d_f$, respectively. Inset: $\langle R(s)^2 \rangle$ vs s at the critical point.

Hexagon	Initial Sites	Hexagon	Initial Sites
$\alpha, -\delta, \beta$	(2, 0, 2) (2, -2, 4)	$\alpha, -\gamma, \delta$	(0, 0, 0) (0, -2, 2)
$\delta, -\gamma, \beta$	(4, 2, 2) (4, 4, 4)	$\alpha, -\beta, \gamma$	(4, 2, 2) (4, 4, 4)

TABLE I: hexagons and their initial sites in the unit cell.

very long trajectories, which can be generated individually in samples of unbounded size. We class a trajectory as long if it has not closed on itself after 5×10^7 steps, and we analyse behaviour for the first 10^7 steps. At $p = p_c$ we expect to see with this method the fractal behaviour of critical walks, and in the inset to Fig. 3 we show that $\langle R(s)^2 \rangle$ varies as a power of s . From this we extract $2/d_f = 0.784 \pm 0.004$, which is consistent with the value determined from τ using Eq. (9). In the extended phase we expect scaling collapse of $\langle R(s)^2 \rangle / \xi(p)^2$ plotted as a function of $s / \xi(p)^{d_f}$ for different p . This is illustrated in the main panel of Fig. 3 using four values of p . Two power law regimes are apparent: $\langle R(s)^2 \rangle \sim s^{2/d_f}$ for small $s / \xi(p)^{d_f}$, as at the critical point; and $\langle R(s)^2 \rangle \sim s$ for large $s / \xi(p)^{d_f}$, as for free random walks.

We close with a full description of our model, deferred above. Consider a diamond lattice. We take as Cartesian coordinates for the two sites in the primitive unit cell: $\mathbf{r} = (0, 0, 0)$ on sublattice A , and $\mathbf{r} = (1, 1, 1)$ on sublattice B . At an A -site the position vectors to neighbouring B -sites are: $\alpha = (1, 1, 1)$, $\beta = (-1, -1, 1)$, $\gamma = (-1, 1, -1)$ and $\delta = (1, -1, -1)$. For $p = 0$ all classical paths in the model are closed hexagons. They can be specified by giving an initial site and the first three steps. The unit cell of the model consists of such eight hexagons, as listed in Table 1. The model does

not retain the full point symmetry of the diamond lattice, being instead tetragonal. It is, however, not very anisotropic: the ratio of conductivities in the two distinct directions is about 1.1 and depends very little on p .

In conclusion, we have used the mapping to classical walks as a means to investigate the three-dimensional class C localisation transition with high precision. Possible future extensions include the study of two and three particle Green functions [18] and of lattices with higher coordination number [19]. Most importantly, an analytical understanding of the classical problem, perhaps based on ideas from polymer physics [20], would be very desirable.

This work was supported by EPSRC Grant No. EP/D050952/1, by DGI Grant No. FIS2006-11126, and by Fundacion Seneca, Grant No. 03105/PI/05.

-
- [1] F. Evers and A. D. Mirlin, *Rev. Mod. Phys.* **80**, 1355 (2008).
 - [2] I. A. Gruzberg, A. W. W. Ludwig, and N. Read, *Phys. Rev. Lett.* **82**, 4524 (1999).
 - [3] E. J. Beamond, J. Cardy, and J. T. Chalker, *Phys. Rev. B* **65**, 214301 (2002).
 - [4] A. Altland and M. R. Zirnbauer, *Phys. Rev. B* **55**, 1142 (1997); M. R. Zirnbauer, *J. Math. Phys.* **37**, 4986 (1996).
 - [5] T. Senthil *et al.*, *Phys. Rev. Lett.* **81**, 4704 (1998); T. Senthil and M. P. A. Fisher, *Phys. Rev. B* **60**, 6893 (1999).
 - [6] R. Bundschuh *et al.*, *Phys. Rev. B* **59**, 4382 (1999); A. Altland, B. D. Simons, and M. R. Zirnbauer, *Phys. Rep.* **359**, 283 (2002).
 - [7] P. W. Brouwer *et al.*, *Phys. Rev. Lett.* **85**, 1064 (2000); M. Titov *et al.*, *Phys. Rev. B* **63**, 235318 (2001).
 - [8] J. T. Chalker and P. D. Coddington, *J. Phys. C* **21**, 2665 (1988).
 - [9] V. Kagalovsky, B. Horovitz, and Y. Avishai, *Phys. Rev. B* **55**, 7761 (1997); V. Kagalovsky, B. Horovitz, Y. Avishai, and J. T. Chalker, *Phys. Rev. Lett.* **82**, 3516 (1999).
 - [10] F. Evers, A. Mildenerger, and A. D. Mirlin, *Phys. Rev. B* **64**, 241303(R) (2001).
 - [11] O. Schenk, M. Bollhöfer, and R. A. Römer, *SIAM J. Sci. Comp.* **28**, 963 (2006).
 - [12] J. Brndiar and P. Markos, *Phys. Rev. B* **74**, 153103 (2006).
 - [13] K. Slevin and T. Ohtsuki, *Phys. Rev. Lett.* **82**, 382 (1999); *Phys. Rev. B* **63**, 045108 (2001).
 - [14] J.-L. Pichard and G. Sarma, *J. Phys. C* **14**, L127 (1981); A. MacKinnon and B. Kramer, *Z. Phys.* **53**, 1 (1983).
 - [15] Ch. 15 in *Numerical Recipes in Fortran*, W. Press, B. Flannery, and S. Teukolsky (Cambridge University Press, 1992).
 - [16] V. Kagalovsky, B. Horovitz, and Y. Avishai, *Phys. Rev. Lett.* **93**, 246802 (2004).
 - [17] A. W. W. Ludwig, private communication.
 - [18] A. D. Mirlin, F. Evers, and A. Mildenerger, *J. Phys. A* **36**, 3255 (2003).
 - [19] J. L. Cardy, *Comm. Math. Phys.* **258**, 87 (2005).
 - [20] P. G. de Gennes, *Phys. Lett.* **38A**, 339 (1972).